1 **SUPPLEMENTARY TABLES AND TABLE LEGENDS**

2 **Table S1. Differential expression matrix utilized in single-cell RNA sequencing data**

3 **analysis to identify cell clusters, Related to Figure 1.**

4

5 **Table S2. Differential expression of genes between ccRCC tumor cluster and normal**

6 **epithelium cluster, Related to Figure 1.**

7

8 **Table S3. List of oligonucleotides used for qPCR.**

Gene	Forward primer	Reverse primer
ACAD9	TCGGAGATGGGTTTAAGGTG	CGTAAGCCTTCTGAGCCATC
ACOT7	CCGAAAACATCCTCACAGGT	GTTCCTCCACTTGGTCTCCA
APOE	GGTCGCTTTTGGGATTACCT	TCCAGTTCCGATTTGTAGGC
β-Actin	CATGTACGTTGCTATCCAGG	CTCCTTAATGTCACGCACGAT
CPT1A	GAAGATGGCAGAAGCTCACC	TGGCGTACATCGTTGTCAT
DBI	TGGCCACTACAAACAAGCAA	TGGCACAGTAACCAAATCCA
EPAS1	GACATGAAGTTCACCTACTGTGATG	CGGAGTCTAGCGCATGGTA
FABP7	CCAGCTGGGAGAAGAGTTTG	CTCATAGTGGCGAACAGCAA
HIF1a	CAGCTATTTGCGTGTGAGGA	TTCATCTGTGCTTTCATGTCATC
IGFBP3	CAGAGACTCGAGCACAGCAC	GATGACCGGGGTTTAAAGGT
LOX	GGACTGAGAAAGGGGAAAGG	GGACGTGGCTCACAGAAAAT
PLIN4	CAGATGCAGGAAGCATCAAA	GCGACTAAAAGGCACTCTGG
RARRES2	GTGCAAAGTCAGGCCCAATG	TTGGGTCTCTATGGGGCAGT
RORC	CAGTGAGAGCCCAGAAGGAC	TCATCCCATCCATTTTTGGT
SMPD3	GAGGGCTGCATCTCTACCAG	ACCCTGTGAAGTGAGGGTTG
VEGFA	TCCTCACACCATTGAAACCA	GATCCTGCCCTGTCTCTCTG

9

10 **Table S4. List of recombinant DNAs.**

TRCN Name	Name in Manuscript	Gene Name
TRCN0000063443	shRARRES2-1	RARRES2
TRCN0000373361	shRARRES2-2	RARRES2
TRCN0000373359	shRARRES2-3	RARRES2
TRCN0000003803	shHIF2α	EPAS1

11

siGENOME SMARTpool siRNA	Gene Name	Target Sequence
M-021441-01	KLF6	GCCUAGAGCUGGAACGUUA
M-021441-02	KLF6	GCAGGAAAGUUUACACCAA
M-021441-03	KLF6	UGCAAGAAGUGAUGAGUUA
M-021441-04	KLF6	AAAUUGAGCUCCUCUGUCA

12

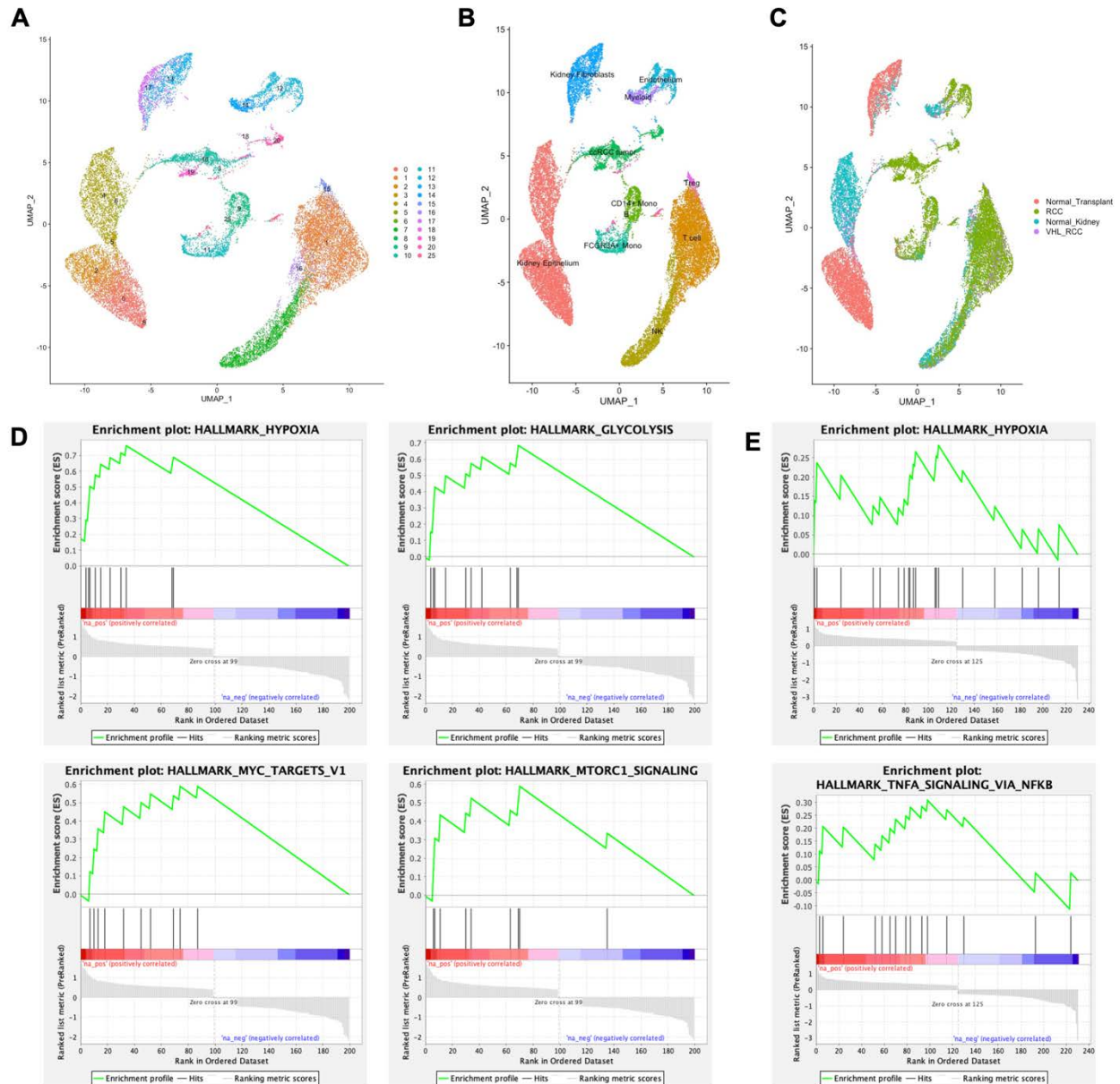**Table S5. List of noncoding guide RNAs for CRISPR-Cas9.**

Gene number	Sequence
RARRES2 A1	5'-CACCGGACCAGTGTGGAGAGCGCCG-3'
RARRES2 A2	5'-AAACCGGCGCTCTCCACACTGGTCC-3'
RARRES2 B1	5'-CACCG GCGACGGCTGCTGATCCCTC-3'
RARRES2 B2	5'-AAACGAGGGATCAGCAGCCGTCGCC-3'
RARRES2 C1	5'-CACCG CTATGGGGCAGTGGACCAAC-3'
RARRES2 C2	5'-AAACGTTGGTCCACTGCCCCATAGC-3'
RARRES2 D1	5'-CACCG CCAGTGCTGGCTTAGCTGCG-3'
RARRES2 D2	5'- AAACCGCAGCTAAGCCAGCACTGGC-3'
RARRES2 E1	5'-CACCG CCCTTCTTACCCGCAGAACT-3'
RARRES2 E2	5'-AAACAGTTCTGCGGGTAAGAAGGGC-3'
RARRES2 F1	5'- CACCG ATTGGGCCTGACTTTGCACT-3'
RARRES2 F2	5'- AAACAGTGCAAAGTCAGGCCCAATC-3
CMKLR1 F1	5'-CACCGGAACCACCGCAGCGTTCGCC-3'
CMKLR1 R1	5'-AAACGGCGAACGCTGCGGTGGTTCC-3'
CMKLR1 F2	5'-CACCGCAAACTGCAGCGCAACCGCC-3'
CMKLR1 R2	5'-AAACGGCGGTTGCGCTGCAGTTTGC-3'
CMKLR1 F3	5'-CACCGTGTGGGGTATAGCCGGCACA-3'
CMKLR1 R3	5'-AAACTGTGCCGGCTATACCCCACAC-3'
CMKLR1 F4	5'-CACCGCCATATCACCTATGCCGCCA-3'
CMKLR1 R4	5'-AAACTGGCGGCATAGGTGATATGGC-3'
CMKLR1 F5	5'-CACCGGTATTCATCACCGTAACTGA-3'
CMKLR1 R5	5'-AAACTCAGTTACGGTGATGAATACC-3'
CMKLR1 F6	5'-CACCGGCGCTGCAGTTTGCACACGA-3'
CMKLR1 R6	5'-AAACTCGTGTGCAAACTGCAGCGCC-3'

14

Table S6. List of antibodies.

Antibodies	Source	Catalog Number
Rabbit anti-RARRES2 (IB) (Polyclonal)	Proteintech	Cat# 10216-1-AP
Rabbit anti-EPAS	Novus	Cat# NB100-122
Mouse ant-β-Actin (Monoclonal)	Sigma-Aldrich	Cat# A1987
Mouse anti-NDUFA9 (Monoclonal)	Abcam	Cat# ab14713
Mouse anti-UQCRC2 (Monoclonal)	Abcam	Cat# ab14745
Mouse anti-COX1 (Monoclonal)	Abcam	Cat# ab14705
Rabbit anti-SDHA (Polyclonal)	Proteintech	Cat# 14865-1-AP
Mouse anti-ATP5A (Monoclonal)	Abcam	Cat# ab14748
Rabbit anti-VHL (Polyclonal)	Cell signaling	Cat# 2738S
Rabbit anti-p-Akt Ser473 (Polyclonal)	Cell signaling	Cat# 9271S
Rabbit anti-p-Akt Thr308 (Polyclonal)	Cell signaling	Cat# 9275S
Rabbit anti-Akt (Polyclonal)	Cell signaling	Cat# 9272S
Rabbit anti-p-p44/42 MAPK Thr202/Tyr204 (Polyclonal)	Cell signaling	Cat# 9101S

15

|		
Rabbit anti-p44/42 MAPK (Polyclonal)	Cell signaling	Cat# 9102S
Mouse anti-KLF6, clone 12A.8.3 (Monoclonal)	Millipore-Sigma	Cat# MABN119
Mouse anti-CMKLR1 (ChemR23, C-7) (Monoclonal)	Santa Cruz	Cat# sc-374570
Rabbit anti-RARRES2 (Polyclonal) (IHC)	Phoenix Pharmaceuticals	Cat# H-002-52
Mouse Gamma Globulin	Jackson Immuno Research	Cat# 015-000-002
Anti-RARRES2 (Monoclonal)	BioXCell	MMC-Rarres2-1H1

16

SUPPLEMENTARY FIGURES AND FIGURE LEGENDS

18

Figure S1. Cells are classified into different cell clusters and display distinctive gene signatures, Related to Figure 1.

Heatmap displays the differentially expressed genes in each cluster of cell populations identified from single-cell RNA-sequencing. The differentially expressed genes were utilized to identify cell populations (Supplementary Table S1). Purple, low expression; yellow, high expression.

24

Figure S2. ccRCC tumor cluster shows specific tumor gene signatures, as compared to other cell clusters, Related to Figure 1.

(A)   Uniform manifold approximation and projection (UMAP) includes all cells from normal transplant kidney, ccRCC tumors, normal adjacent kidney tissues and wild-type VHL ccRCC tumors. Tumors cluster annotations according to gene markers from scRNA-seq in Supplementary Figure S1.

31   (B)   The same UMAP as in (A) with selected cell types annotated; the cell types were

32   determined according to the expression level of the representative gene markers indicated

33   in Supplementary Figure S1.

34   (C)   The cluster annotations according to the tissue types.

35   (D)   Gene set enrichment analysis verifies the upregulation of hypoxia, glycolysis, myc-targets

36   and mTORC1 signaling related genes in ccRCC tumor clusters as compared to epithelium.

37   Purple, low expression; red, high expression.

38   (E)   Gene set enrichment analysis shows no significant correlation of hypoxia and NFKB

39   related genes between two subclusters of ccRCC tumor cells. Purple, low expression; red,

40   high expression.

41
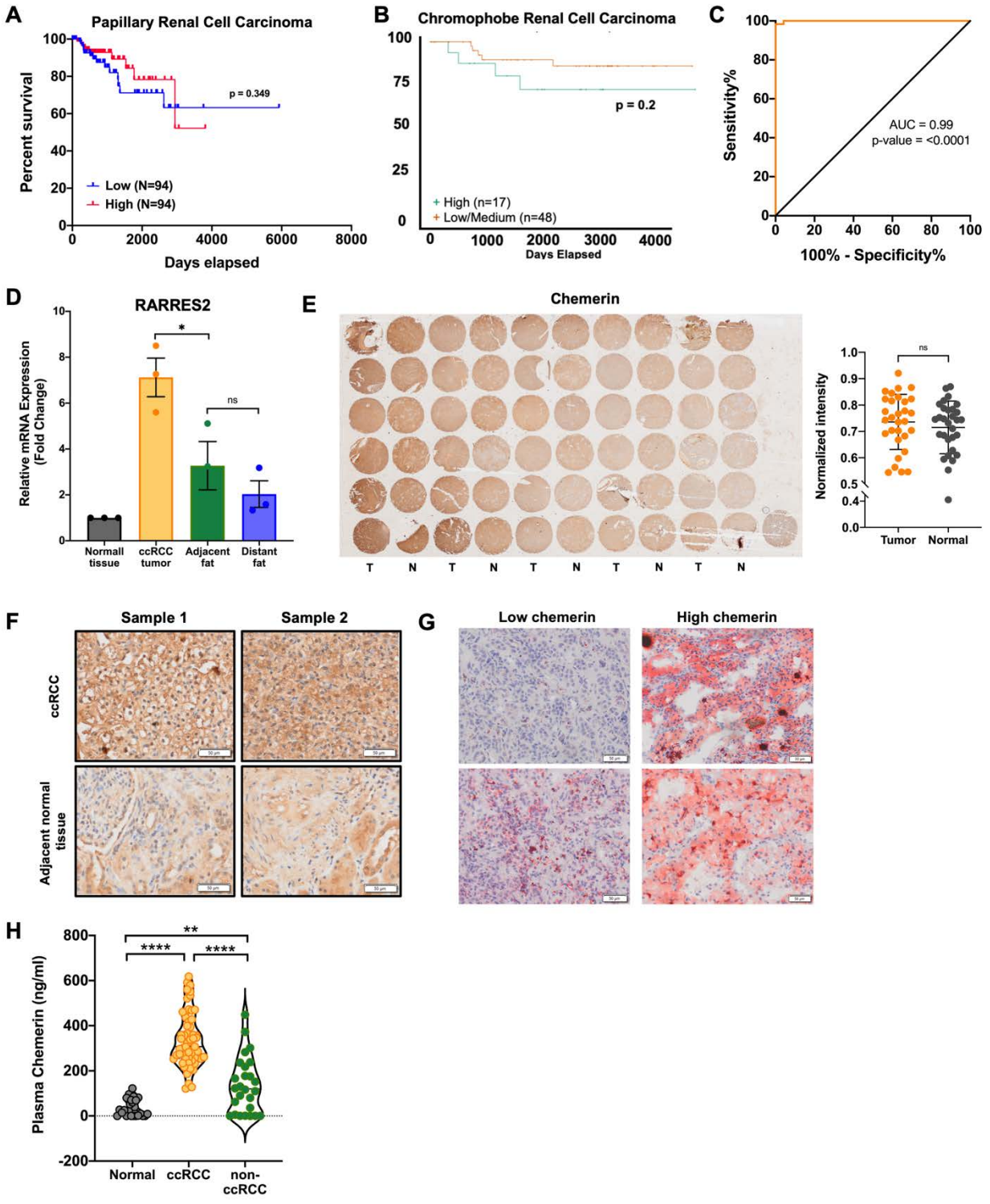
Figure S3. Chemerin protein is detected in ccRCC tissue; and chemerin expression is not correlated with survival of patients with papillary renal cell carcinoma and chromophobe renal cell carcinoma, Related to Figure 1.

45 (A) Kaplan-Meier curve showing no correlation of higher mRNA expression of chemerin with

46   survival of papillary renal cell carcinoma patients in the TCGA KIRP dataset using upper

47   and lower third cohorts. Log rank analysis.

48 (B) Kaplan-Meier curve showing no correlation of higher mRNA expression of chemerin with

49   survival of chromophobe renal cell carcinoma patients in the TCGA KICH dataset using

50   upper and lower third cohorts. Log rank analysis.

51 (C) ROC curve of plasma chemerin. Area under the curve is 0.99 with sensitivity of 98.31%

52   and specificity of 95.83% at the cut-off value of 121.6 ng/mL.

53 (D) Relative expression of chemerin in normal kidney tissue adjacent to ccRCC tumor, ccRCC

54   tumor tissue, fat tissue adjacent to the ccRCC tumor tissue, and fat tissue distant to the

55   ccRCC tumor tissue. Two-tailed student's t-test.

56 (E) Immunohistochemistry staining (IHC) of chemerin protein expression in a tumor

57   microarray containing 30 ccRCC tissues with matched cancer adjacent kidney tissue.

58   Each column represents different pairs of tumor (T) and normal (N) samples. Normalized

59   intensity of staining was quantified on the right.

60 (F) Representative 10× pictures of ccRCC and normal adjacent kidney tissues in IHC sections

61   in (E).

62 (G) Representative Oil-Red-O pictures of ccRCC with low and high expression of chemerin

63   (10×).

64 (H) Plasma chemerin concentration in normal healthy individuals (n=24), patients with ccRCC

65   tumor (n=59) and patients with papillary RCC (non-ccRCC) (n=26). Mann-Whitney U-test.

66 Error bars represent SD. $*p < 0.05$; $**p < 0.01$; $***p < 0.001$; $**** p < 0.0001$.

67
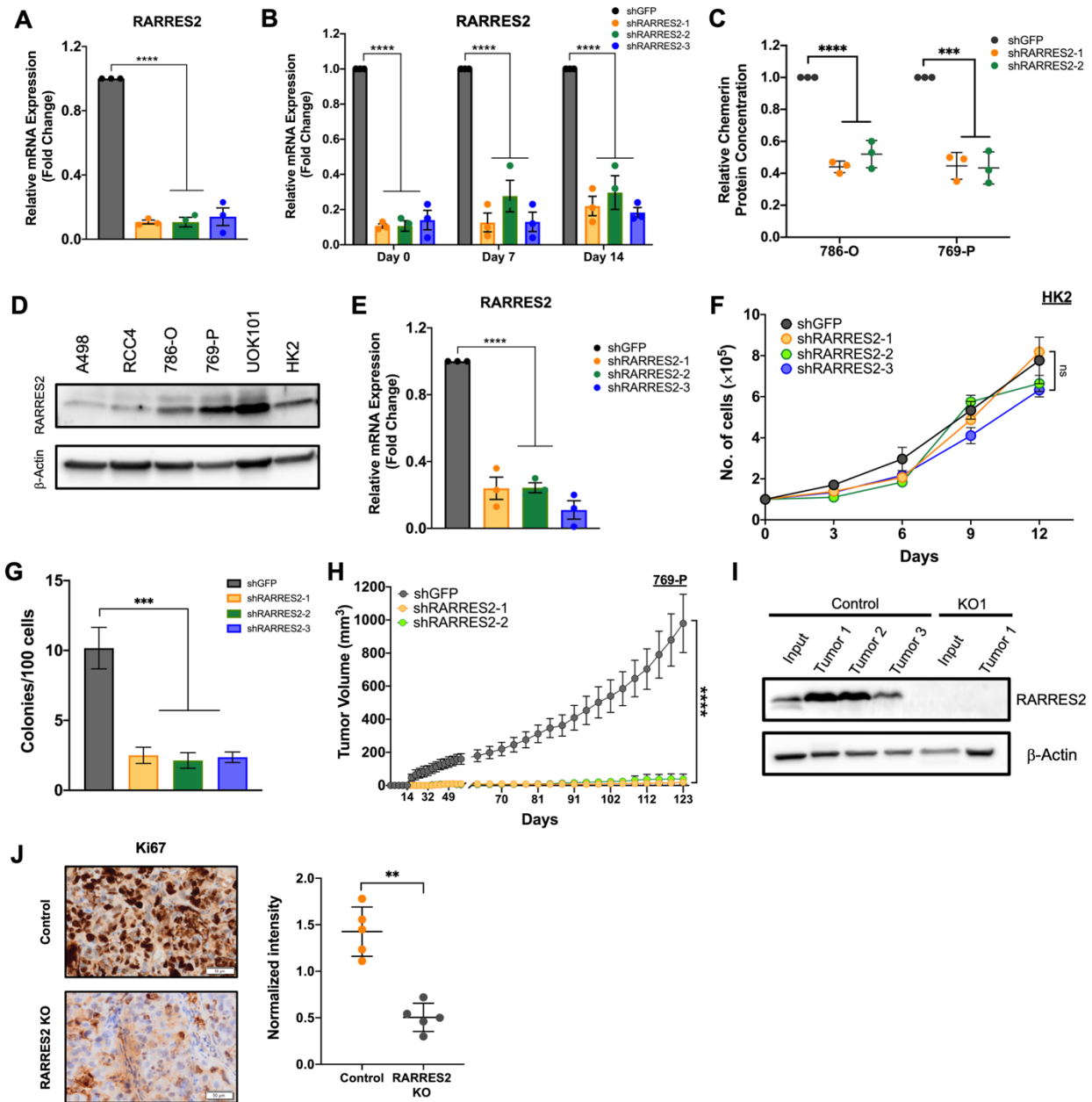
Figure S4. Chemerin is functionally important for ccRCC growth, Related to Figure 2.

(A)   Relative mRNA expression of chemerin in 786-O following knockdown with 3 independent,

        non-overlapping   shRNAs   targeting   RARRES2   (shRARRES2-1,   shRARRES2-2,

        shRARRES2-3) or control shGFP. One-way ANOVA.

(B)   Relative mRNA expression of chemerin in 786-O following knockdown with 3 independent,

        non-overlapping   shRNAs   targeting   RARRES2   (shRARRES2-1,   shRARRES2-2,

| 74 | | shRARRES2-3) or control shGFP at Day 0, Day 7 and Day 14 post-infection. One-way |
75		ANOVA.
76	(C)	Relative chemerin protein concentration in media of 786-O and 769-O following
77		knockdown with 3 independent, non-overlapping shRNAs targeting RARRES2
78		(shRARRES2-1, shRARRES2-2, shRARRES2-3) or control shGFP 72 hours post-
79		infection. One-way ANOVA. Error bars represent SD.
80	(D)	Immunoblot of different ccRCC cell lines (A-498, RCC4, 786-O, 769-P, UOK101 and HK-
81		2) demonstrating relative chemerin protein expression.
82	(E)	Relative mRNA expression of chemerin in HK-2 following knockdown with 3 independent,
83		non-overlapping shRNAs targeting RARRES2 (shRARRES2-1, shRARRES2-2,
84		shRARRES2-3) or control shGFP. One-way ANOVA.
85	(F)	Cell proliferation assay from HK-2 cells infected with shGFP control or 3 different shRNAs
86		encoding lentivirus targeting chemerin (shRARRES2-1, shRARRES2-2, shRARRES2-3).
87		Two-way repeated measures ANOVA with Geisser-Greenhouse correction.
88	(G)	Colony forming assay from 786-O cells infected with shGFP control or 3 different shRNAs
89		encoding lentivirus targeting chemerin (shRARRES2-1, shRARRES2-2, shRARRES2-3),
90		measured by number of colonies formed from initial 100 cells after 2 weeks. Two-way
91		repeated measures ANOVA with Geisser-Greenhouse correction.
92	(H)	Subcutaneous tumor volume measurement in nude mice implanted with 769-P cells which
93		were infected with lentivirus encoding either shGFP (n=8) or 2 different shRARRES2 (n=8
94		in each arm). Two-way measures ANOVA with Dunnett's multiple comparison test
95		correction.
96	(I)	Immunoblot of subcutaneous tumors derived from sgCONT and sgRARRES2 from Fig.
97		2G demonstrating complete knockout of chemerin protein.

98   (J)   Ki67 IHC of subcutaneous tumors derived from sgCONT and sgRARRES2 from Fig. 2G

99   demonstrating reduced tumor cell proliferation *in vivo* (10×). Representative images were

100   quantified and shown on the right.

101   Error bars represent SEM of three independent experiments and three technical replica per

102   experiment. $*p<0.05$, $**p<0.01$, $***p<0.001$, $****p<0.0001$.

103

104

Figure S5. Lipid metabolism pathways alteration in chemerin-deficient ccRCC, Related to

Figure 3.

107   (A)   Volcano plot showing commonly differentially expressed genes in between 786-O cells

108   infected with lentivirus encoding either shGFP control (n=3) or combined shRARRES2

109   clones (n=8).

110   (B)   Heatmaps showing the downregulated genes in chemerin-targeted versus control 786-O

111   cells in different lipid metabolism pathways. Purple, low expression; red, high expression.

112   (C)   Representative EdU flow cytometry plots for Fig. 3G.

113   (D)   50 µM Etomoxir treatment rescues proliferation defect in chemerin-knockdown 786-O cells,

114   measured by cell proliferation assay. Two-way repeated measures ANOVA with Geisser-

115   Greenhouse correction.

116   Error bars represent SD. $*p<0.05$, $**p<0.01$, $***p<0.001$, $****p<0.0001$.

117

Figure S6. Untargeted lipidomics profiling in 786-O with chemerin inhibition, Related to

Figure 4.

120   (A)   Overview of lipid profiles between two independent clones of shRARRSE2 obtained

121   through untargeted lipidomic analysis as annotated by the LipidMatch (guided in-source

122   fragment annotation) algorithm.

123   (B)   Clustering between control and two independent clones of shRARRSE2 obtained through

124   untargeted lipidomic analysis as annotated by the LipidMatch (Based on MS/MS based

125   confirmation) algorithm.

126   (C)   Percentage of each lipid species identified in mass spectrometry analysis.

127   (D)   The lipid species identified in intact and oxidized/breakdown lipid categories.

128   (E)   Structure of phosphatidylcholine (PC) and lysophosphatidylcholine (LPC).

129   (F)   Heatmap from untargeted lipidomics showing lower sphingomyelin species and increased

130   breakdown product sphingosine in chemerin deficient cells. Blue, low expression; red, high

131   expression. DG, diacylglcerols; SM, sphingomyelin; So, sphingosine.

132   (G)   Heatmap from untargeted lipidomics showing reduction in glycerolipid

133   monogalactosyldiacylglycerol (MGDG) in chemerin deficient cells. Blue, low expression;

134   red, high expression. MG, monoglyceride; MGDG, monogalactosyldiacylglycerol.

135
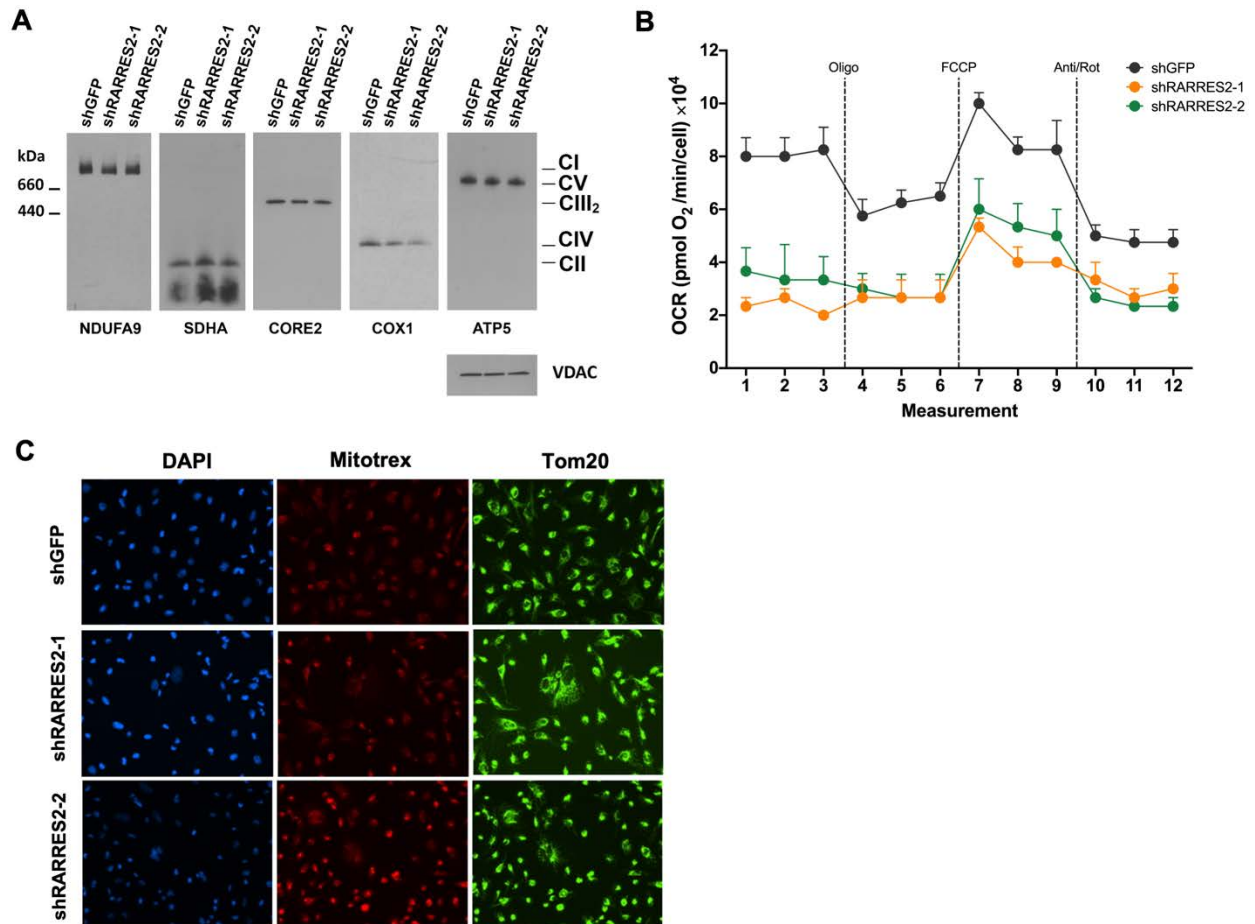
Figure S7. Chemerin inhibition reduces mitochondrial OXPHOS complex IV but do not cause overall structural change to mitochondria, Related to Figure 5.

(A)   Steady-state levels of mitochondrial individual OXPHOS complex III subunit CORE2 and complex IV subunit COX1 in 786-O cells infected with lentivirus targeting shGFP or 2 different shRARRES2. This was evaluated by BN-PAGE analysis of whole cell extracts prepared in the presence of 1% lauryl maltoside (LM) and probed with antibodies. Four technical replicates were performed.

(B)   Seahorse Cell Mito Stress Test in 786-O following knockdown with 2 independent, non-overlapping shRNAs targeting RARRES2 (shRARRES2-1, shRARRES2-2) or control shGFP. The oxygen consumption rate (OCR) in chemerin-silenced cell is lower than in the control cell.

147　(C)　Confocal imaging of mitochondrial structure stained with Mitotrex and Tom20 in 786-O

148　　　cells infected with lentivirus targeting shGFP or 2 different shRARRES2 (10×).

149　Error bars represent SD. *p<0.05, **p<0.01, ***p<0.001, ****p<0.0001.

150
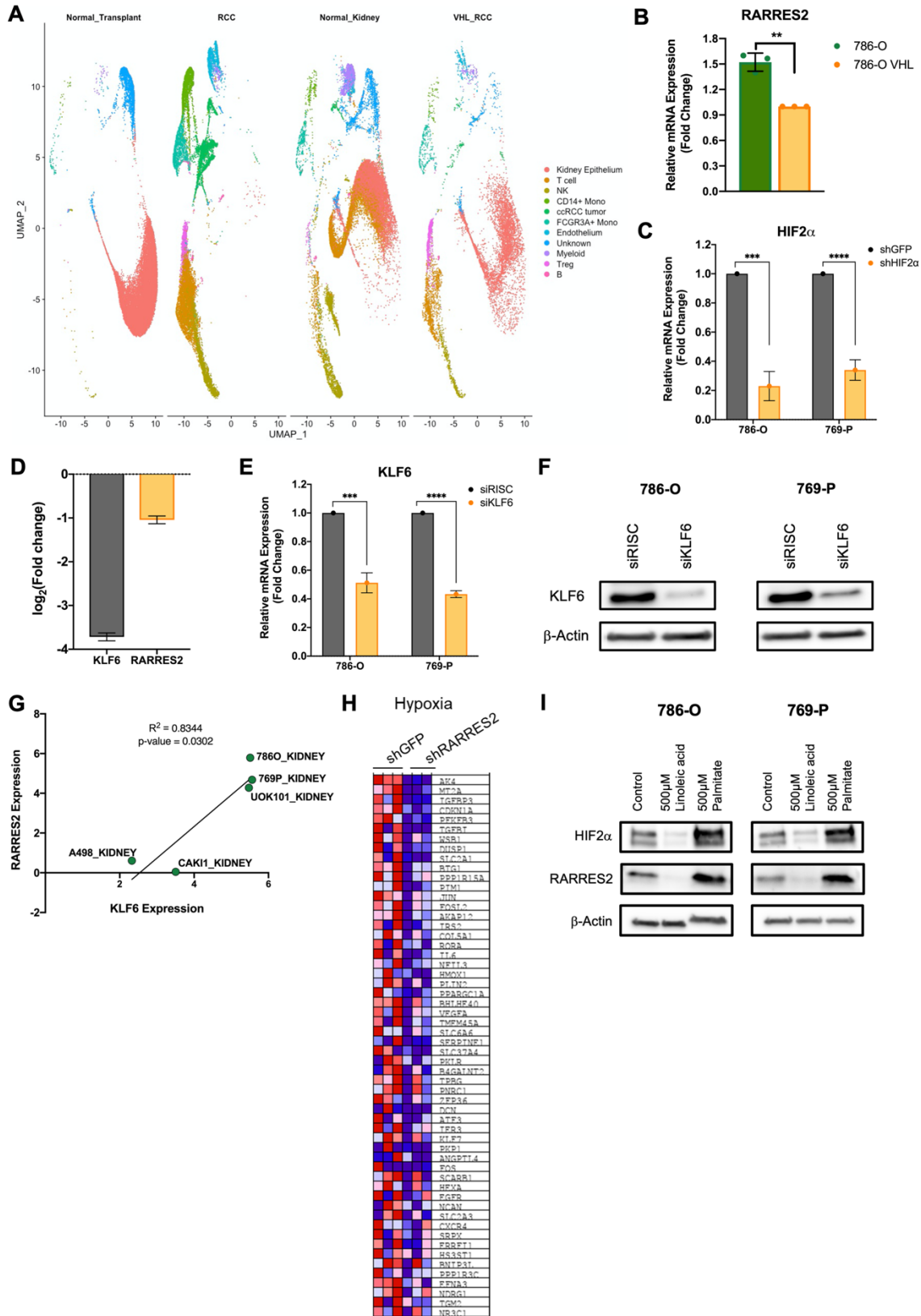
Figure S8. Chemerin regulation by KLF6, Related to Figure 6.

152 (A)   Tumor clusters of human normal kidney, ccRCC specimens with wild-type VHL and
153   ccRCC specimens with VHL mutation from scRNA-seq data, presented as UMAP plots.

154 (B)   Relative mRNA expression of *RARRES2* in 786-O and 786-O VHL cells, measured by
155   qRT-PCR. Two-tailed student's t-test.

156 (C)   Relative mRNA expression of *HIF2α* in 786-O and 769-P cells infected with shGFP control
157   or shRNAs encoding lentivirus targeting HIF2α, confirming knockdown of HIF2α in Fig.
158   6C. Two-tailed student's t-test.

159 (D)   Fold change of *RARRES2* mRNA expression in 786-O with KLF6 knockdown as
160   compared to control, extracted from RNA-seq data (28).

161 (E)   Relative mRNA expression of *KLF6* in 786-O and 769-P cells transfected with control
162   siRISC or siRNA targeting KLF6 (siKLF6), confirming knockdown of KLF6 in Fig. 6D. Two-
163   tailed student's t-test.

164 (F)   Immunoblot of lysate confirming knockdown of KLF6 in 786-O and 769-P cells transfected
165   with control siRISC or siKLF6 in Fig. 6D.

166 (G)   Correlation of chemerin and KLF6 expression in multiple ccRCC cell lines interrogated
167   from the Cancer Dependency Map database. The R^2 value of the linear correlation is 0.83
168   with p-value of 0.0302.

169 (H)   Heatmap of downregulated hypoxia pathway genes in 786-O infected with lentivirus
170   encoding either shGFP or shRARRES2. Purple, low expression; red, high expression.

171 (I)   Immunoblots of lysates of 786-O and 769-P cells treated with 500 μM linoleic acid (a
172   polyunsaturated fatty acid) or 500 μM palmitate (a saturated fatty acid), showing
173   decreased in HIF2α and chemerin protein after incubation with 500 μM linoleic acid but
174   increased after incubation with 500 μM palmitate.

175 Error bars represent SEM. *p<0.05, **p<0.01, ***p<0.001, ****p<0.0001.

176
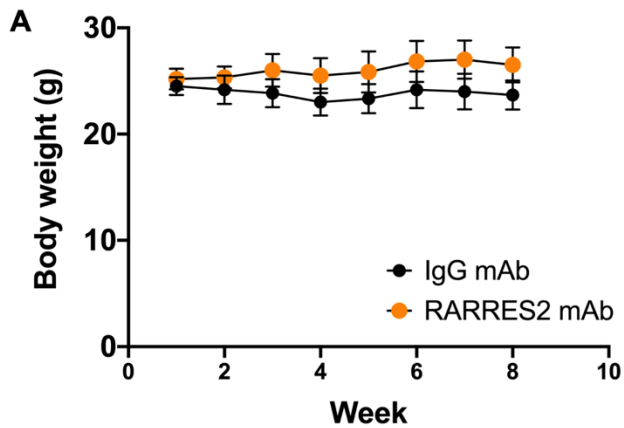
Figure S9. Monoclonal antibody targeting chemerin shows no toxicity in mice, Related to Figure 7.

(A)   The weight of mice receiving 20mg/kg of either mAb (n=6 each arm), after 786-O was implanted orthotopically under the left kidney capsule of nude mice. Weight is recorded weekly starting from the day of tumor implantation.
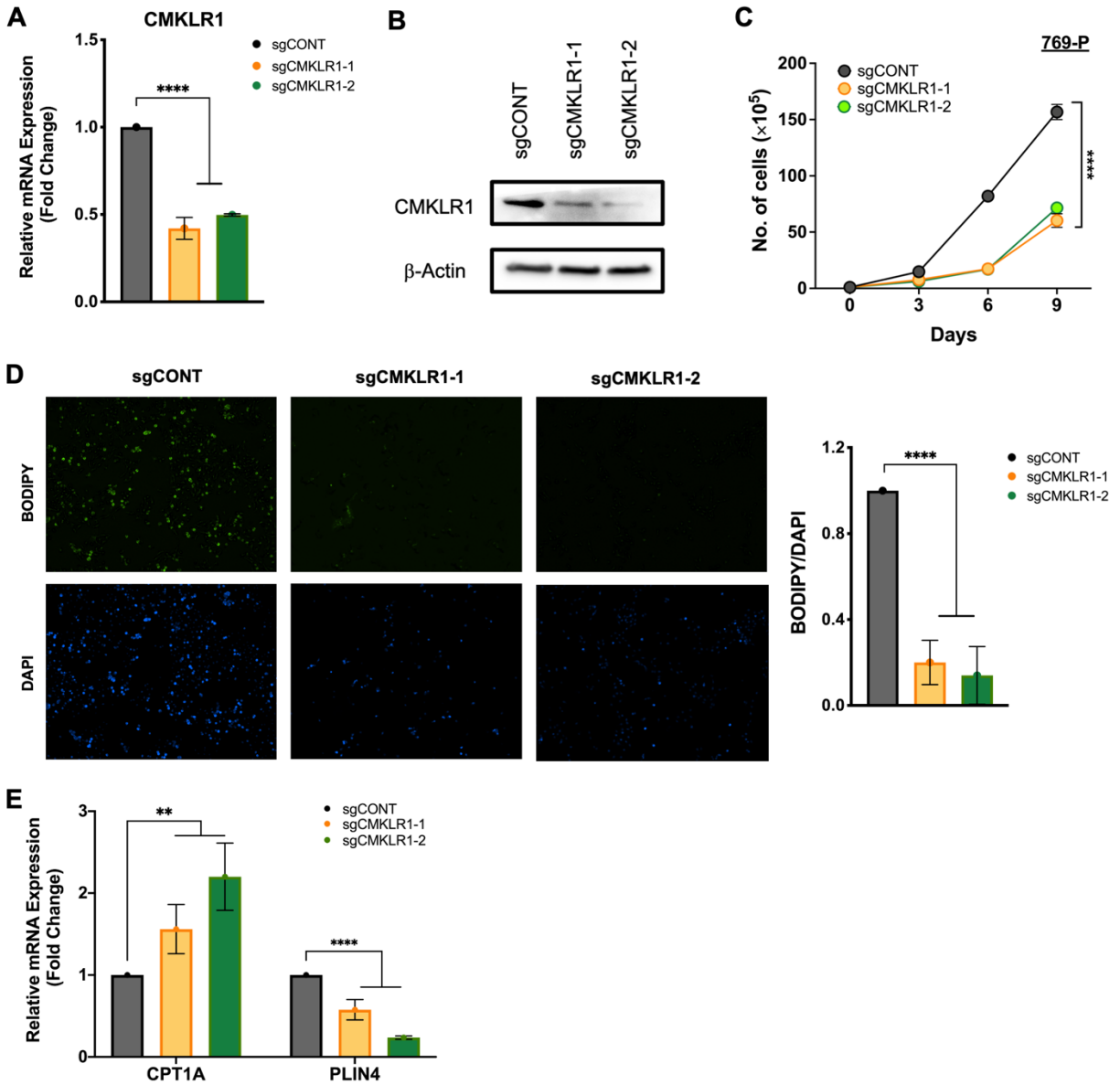
Figure S10. CMKLR1 regulates cell growth and lipid metabolism in ccRCC cells.

(A) Relative mRNA expression of CMKLR1 in 769-P cell infected with lentivirus encoding either control sgCONT or sgCMKLR1 (sgCMKLR1-1 and sgCMKLR1-2). Two-way repeated measures ANOVA with Geisser-Greenhouse correction.

(B) Immunoblot of lysate confirming knockdown of CMKLR1 protein from 769-P cells infected with sgCONT or sgCMKLR1 (sgCMKLR1-1 and sgCMKLR1-2).

189   (C)   Cell proliferation assay of 769-P cells infected with lentivirus encoding either sgCONT or

190   sgCMKLR1 (sgCMKLR1-1 and sgCMKLR1-2). Two-way repeated measures ANOVA with

191   Geisser-Greenhouse correction.

192   (D)   BODIPY staining of 769-P cells infected with either sgCONT or sgCMKLR1 (sgCMKLR1-

193   1 and sgCMKLR1-2) (upper panel). DAPI staining of nucleus in lower panel (4×).

194   Quantification of BODIPY staining, normalized to DAPI staining in 769-P cells infected

195   with lentivirus encoding either sgCONT or sgCMKLR1 (sgCMKLR1-1 and sgCMKLR1-2).

196   One-way ANOVA.

197   (E)   Expression of CPT1A and PLIN4, as measured by qRT-PCR, in the 769-P cells infected

198   with either sgCONT or sgCMKLR1 (sgCMKLR1-1 and sgCMKLR1-2). One-way ANOVA.

199   Error bars represent SD. *$p < 0.05$, **$p < 0.01$, ***$p < 0.001$, ****$p < 0.0001$.